Materials Research. 2017; 20(6): 1593-1599
DOI: http://dx.doi.org/10.1590/1980-5373-MR-2017-0173

Comparative Study of Microstructure, Texture, and Formability Between 11CrTi and 11CrTi+Nb ASTM 409 Ferritic Stainless Steel

Ricardo José Gonçalves Costa[a], Daniella Gomes Rodrigues[b], Hélio José Batista Alves[a],

Tarcísio Reis de Oliveira[a], Berenice Mendonça Gonzalez[b]*

[a]Research Center, Aperam South America, Timóteo, MG, Brazil.
[b]Department of Metallurgical and Materials Engineering, Universidade Federal de Minas Gerais - UFMG, Belo Horizonte, MG, Brazil.

Received: February 03, 2017; Revised: July 09, 2017; Accepted: August 01, 2017

Stabilization of ferritic stainless steel ASTM 409, for use in automobile exhaust systems, is increasingly in demand, due to higher exhaust gas temperatures. Ti is one of the most commonly used elements. However, high concentrations cause problems during steel casting; however, stabilization with Ti and Nb represents a good alternative. The present study aims to investigate the effect of adding Nb on the microstructure, texture, and forming properties of Ti-stabilized ferritic steels. The results demonstrated that Nb-addition leads to a more deformed microstructure after hot rolling with the strongest {110}⟨001⟩ Goss component. In the deformed state, the steels displayed the α-fiber, but 11CrTi+Nb steel showed a more intense γ-fiber. After annealing, Nb-addition led to an increase in the γ-fiber and in average normal coefficient of anisotropy ($\overline{R}$). Thus, it was demonstrated that the dual stabilization (Ti+Nb) of the ferritic steel was responsible for improving the recrystallization texture and forming proprieties.

Keywords: *Ferritic stainless steels, texture, anisotropy, stabilization.*

1. Introduction

Stainless steels are increasingly gaining ground in the market, due to their versatility, performance, and resistance to corrosion. In the automobile industry, the Ti-stabilized ferritic stainless steel, ASTM 409, was developed over 30 years ago particularly for use in automotive exhaust systems, where it is widely used today[1,2].

With 11% chromium, low concentrations of carbon, and nitrogen and titanium stabilization, the ferritic stainless steel, ASTM 409 (UNS S40910), shows good performance in most applications. In recent years, new designs of exhaust systems have been developed, increasing the service temperature in order to improve the performance of the catalytic converter.

The higher service temperature leads to a more aggressive environment for the material, which requires better corrosion resistance[3]. Higher concentrations of stabilizing elements in the steel are required, to prevent the possibility of sensitization occurrence particularly in the heat affected zone of the welded joint[4,5]. This prevents the material from exhibiting failures resulting from intergranular corrosion[6].

To meet the needs of automakers that have demanded higher levels of stabilization, such as for new applications in motorcycle exhaust systems, higher concentrations of Ti in the steel are required. A stabilized steel, named 11CrTi (UNS S40920), with higher contents of Ti, was developed in order to achieve better corrosion resistance[7]. However, high concentrations of this element compromise steel casting and the surface quality of coils[6].

One good alternative to reduce the titanium content is dual stabilization with Ti and Nb. The alloy design of this dual-stabilized steel, named 11CrTi+Nb (UNS S40930), aims to ensure the adequate properties for its applications, especially in terms of resistance to intergranular corrosion using the relationship: (Ti+Nb) > 0.08 + 8(C+N)[8].

The objective of this study was to compare the microstructure, texture and forming properties of the Ti stabilized (11CrTi) and Ti+Nb stabilized (11CrTi+Nb) ferritic stainless steels during the thermomechanical process.

2. Materials and Methods

The materials analyzed in this study included the following ASTM 409 ferritic stainless steels: (i) 11CrTi steel and (ii) 11CrTi+Nb steel. The chemical compositions of both steels are presented in Table 1.

*e-mail: gonzalez@demet.ufmg.br

Table 1. Chemical composition

	%C	%Cr	%Ni	%Ti	%Nb	%Mn	%Si	% N
11CrTi	0.0067	11.05	0.17	0.17	0.02	0.17	0.46	0.0078
11CrTi+Nb	0.0073	11.00	0.11	0.15	0.06	0.11	0.49	0.0090

Slabs of the two materials were hot rolled to a thickness of 3.0 mm, pickled and cold rolled to final thickness of 1.20 mm (60% of cold reduction), and then annealed at 940ºC, with a soaking time of around of 24 seconds. All the industrial process after continuous casting were similar for both steels.

Microstructure analyses were performed on a longitudinal section of the sheet, with a Leica DMRM light microscope, using the software program Leco IA3001. To reveal the microstructure, Vilella's reagent was used, with an attack time of 50 seconds. The grain size was measured using the three concentric circles method, in accordance with ASTM standard E112/13[9].

The texture of the hot rolled sample after the final annealing was analyzed by Electron Backscattered Diffraction (EBSD) in the longitudinal section, using a PHILIPS XL-30 scanning electron microscope. The step size used was 4 to 8 µm. The data was processed using the TSL/EDAX™ software. The recrystallization was evaluated by Grain Orientation Spread (GOS). This is determined by the mean orientation of the grain and each pixel in the grain, the result is a mean deviation in orientation[10,11]. In this present work, cut off values of GOS≤1° were chosen for recrystallized grains.

The macro-texture was investigated by X-ray diffraction using a Philips X'Pert PRO MPD diffractometer. The analysis was performed on the surface and in the center of the samples. From the incomplete pole figures of (110), (200), and (211), the orientation distribution functions (ODF) were calculated applying the series expansion method, according to Bunge ($l_{max} = 22$)[12]. The orientations were expressed in Euler angles using the Bunge notation.

Tensile tests were performed to determine the average normal ($\overline{R}$ value) and planar (Δr) anisotropy coefficients, on a 15-ton Instron 5583 machine. The $\overline{R}$ value measures resistance to deformation in the thickness of the sheet, while the Δr measures the variation of R along the longitudinal and transverse rolling directions, indicating a tendency to form an earing[13]. The test samples were prepared in accordance with ASTM standard A370/12[14]. The samples were taken in the directions of 0º, 45º, and 90º relative to the rolling direction of the material in accordance with ASTM standard E517[15].

The forming behavior of steels was evaluated by the Swift test method. This test consists of drawing a cylindrical cup from the flat blank, where the diameters increases until the cut-drawing is fractured. In this study, the test was performed using punch 33 mm speed of 600 mm/min and blanks with sizes varying from 64 to78 mm. The blank holder load was 7 kN, and the tests were performed at room temperature using molybdenum disulfide (MoS_2) lubricant on both sides of the sheet. Tests were performed in an Erichsen machine, Model 142/40.

3. Results

3.1. Starting materials - hot rolled sheets

Figure 1 and Figure 2 show the feature of the microstructure and micro-texture of the hot rolled sheets through the orientation and GOS map, where *N.D* is the normal direction and *R.D* is the rolling direction. From Figure 1a, it can be noted that the microstructure and texture were very heterogeneous along the thickness. Near the surface, the microstructure is formed by the fine grains, and the predominate texture was {011}*//N.D.* (shear texture). In the center region, the orientation of the elongated grains were {111}*//N.D.* and {001}*//N.D*. In addition, as can be observed by the GOS map (Fig. 1b), the recovered grains are predominant in the center region and recrystallized grains are in the surface region of the sheet. Fig.2a shows, in 11CrTi+Nb steel, that the microstructure development was more homogeneous but less recrystallized. The grain size near the surface was larger than those displayed for the 11CrTi steel (Fig.1a). The texture consisted of {011}*//N.D.* near the surface region and {111}*//N.D.* and {001}*//N.D* in the center region. Unlike 11CrTi steel, 11CrTi+Nb steel (Fig.2b) presented no recrystallized grains (Fig.1b).

Figure 3 shows the global texture of the hot rolled sheets. In ϕ_2=45º ODF (Fig. 3a) the texture development was the α-fiber, which peaked at the {112}⟨110⟩ component. The

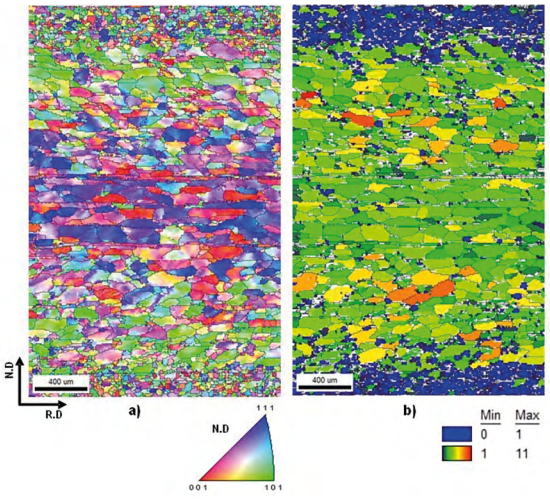

Figure 1. Hot rolled sheet along the thickness of the 11CrTi steel - a) orientation map - b) GOS map.

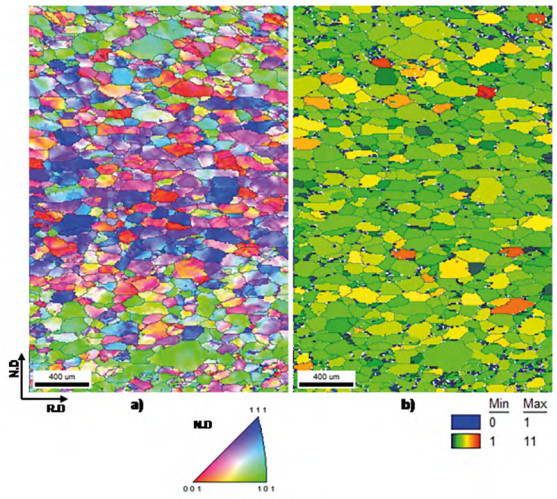

Figure 2. Hot rolled sheet along the thickness of the 11CrTi+Nb steel - a) orientation map - b) GOS map.

maximum *f(g)* occurred at the {110}⟨001⟩ Goss component. As can be seen in 11CrTi+Nb steel (Fig. 3b) the peak occurred at the {110}⟨001⟩ Goss component with *f(g)* ~ 3.6. Among the α-fiber components, the {223}⟨110⟩ was more intense, *f(g)* ~ 1.5. In both sheets of steel, the γ-fiber was poorly developed. Furthermore, it can be noted that the α-fiber was slightly more intense in 11CrTi steel.

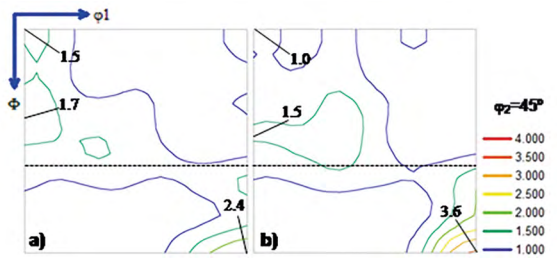

Figure 3. ϕ_2=45º ODF sections of hot rolled sheets - a) 11CrTi steel - b) 11CrTi+Nb steel.

The niobium and titanium contents in the solid solution (ΔNb and ΔTi) were calculated using equations 1, 2[16]. Although it is considered to be single stabilized at Ti, the 11CrTi steel has a residual Nb content which cannot be neglected for the calculation of Ti and Nb in a solid solution. Therefore, the equations used were the same for both steels. The results of the calculations are presented in Table 2.

$$\Delta Ti = \%Ti - 3.42\,\%N - (0.3 \times 4\,\%C) \text{ Dual stabilized steels} \quad (1)$$

$$\Delta Nb = \%Nb - 7.74 \times 0.7\,\%C \text{ Dual stabilized steels} \quad (2)$$

These results show that 11CrTi+Nb steel has a higher amount of niobium in a solid solution than does 11CrTi steel. This can explain the difficulty in the migration of the grain boundaries due to the drag effect (i.e. the difficulty of dragging impurities along the grain boundaries).

Table 2. Calculation of Ti and Nb in solid solution

	%Ti	%Nb	%C	%N	Δ*Nb*	Δ*Ti*
11CrTi	0.17	0.02	0.007	0.008	0	0.134
11CrTi+Nb	0.15	0.06	0.007	0.009	0.022	0.111

3.2. Microstructure and macro-texture of the cold-rolled steels

Figure 4 shows the microstructure along the thickness after cold rolling for both samples. The analyses of the deformed steels have shown a similar microstructure, banded with deformed grains and elongated in the rolling direction, as can be seen in Figures 4a and 4b.

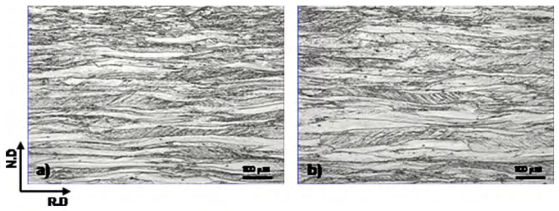

Figure 4. Microstructures after cold-rolling (60% reduction) - a) 11CrTi steel - b) 11CrTi+Nb steel.

Figure 5 shows the ϕ_2=45º ODF sections after the cold rolled process. As can seen in Fig. 5, the macro-texture was heterogeneous along the thickness for both samples. The α-fiber was stronger than the γ-fiber in both regions. However, in the center region, the α-fiber was more intense, reaching a peak at {001}⟨011⟩ in both sheets of steel. Furthermore, the 11CrTi+Nb steel showed a more intense γ-fiber than did the 11CrTi steel in the center region (Fig. 5b and 5d). Among the γ-fibers, the {111}⟨011⟩ was the most developed, *f(g)* = 6.1 (Fig. 5d).

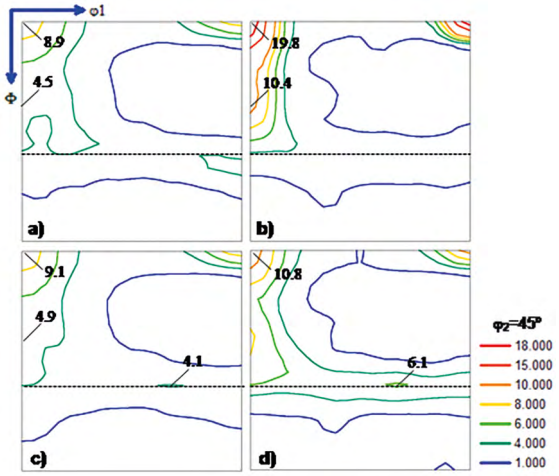

Figure 5. ϕ_2=45º ODF sections of the steels after cold-rolling (60% reduction) - a) surface and b) center of 11CrTi steel; c) surface and d) center of 11CrTi+Nb steel.

3.3. Microstructure and micro-texture after the final annealing of the steels

The microstructures of the materials after annealing are shown in Figure 6 by orientation map. Both sheets of steel have a fully ferritic microstructure and the average grain size was 38 ± 1 µm and 37 ± 1 µm for 11CrTi and 11CrTi+Nb, respectively. As can be seen in Fig. 6b, the 11CrTi+Nb steel exhibited a predominance of grains, with a preferential γ-fiber orientation relative to 11CrTi steel. The volumetric fractions of γ-fiber after annealing were 0.40 and 0.56 for 11CrTi and 11CrTi+Nb steel, respectively. Both sheets of steel showed a small fraction of θ-fiber grains, ({001}//*N.D.*).

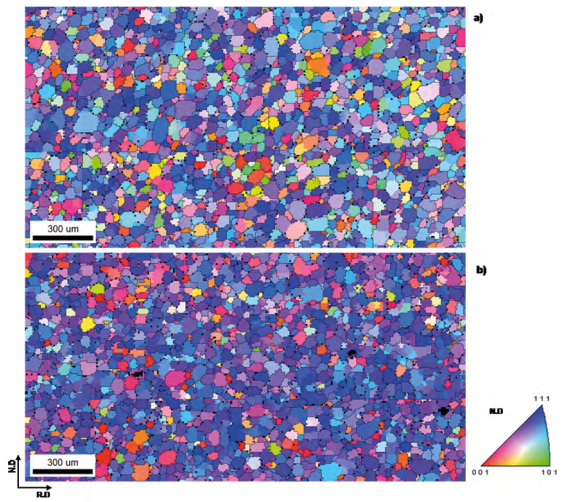

Figure 6. Microstructure and micro-texture after cold rolling and annealing - a) Ti-stabilized steel; b) Ti+Nb-stabilized steel.

Figure 7 shows the ϕ_2=45º ODF sections for both sheets of steel after annealing. From Figure 7a and 7b, it can be noted that the γ-fiber was strongly developed with variable intensity along the φ_1. The maximum in γ-fiber ($f(g)$ = 6.4) occurred at {111}⟨121⟩, Fig. 7b. As can be seen, the shifted components, like {332}⟨113⟩ and {445}⟨334⟩, were developments in both samples. Notice that the θ-fiber and α-fiber were weakly developed.

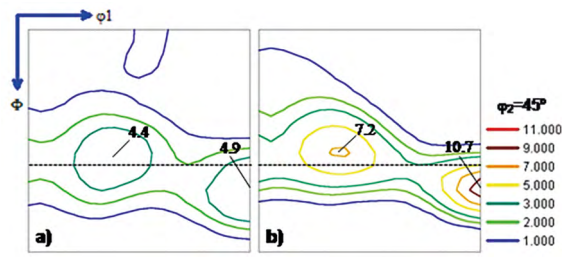

Figure 7. ϕ_2=45º ODF sections. a) Ti-stabilized steel; b) Ti+Nb-stabilized steel.

3.4. Analysis of anisotropy properties

Table 3 shows the results of the average normal and planar coefficient of anisotropy for the two analyzed sheets of steel and γ/θ ratio.

Table 3. Relation of the $\overline{R}$ and planar Δr values and texture

	$\overline{R}$	Δr	γ/θ
11CrTi	1.96	1.34	5.4
11CrTi+Nb	2.09	0.69	8.5

The values obtained show that 11CrTi+Nb steel exhibits better anisotropy results relative to 11CrTi steel. The highest $\overline{R}$ value obtained in 11CrTi+Nb steel indicates a better resistance to deformation in thickness, as compared to 11CrTi steel, favoring a better performance in deep drawing applications.

Figure 8 show the results of the Swift test (LDR- Limit Drawing Ratio) performed on the two sheets of steel. The test results illustrate the better performance of 11CrTi+Nb steel. The values of the planar, Δr, and average normal, $\overline{R}$, anisotropy coefficients are compatible with the lower level of the ears and higher stamping depth achieved.

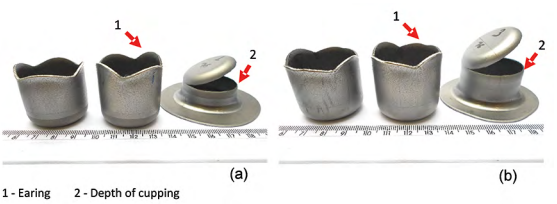

Figure 8. Results of Swift test (LDR) - a) 11CrTi steel; b) 11CrTi+Nb steel.

4. Discussion

The differences in the microstructures of the two steels, shown in Figure 1, are likely to be related to the stronger effect of niobium, compared to titanium, on recrystallization. The presence of niobium is found in a solid solution and in the form of precipitates, and inhibits the displacement of grain boundaries, reducing the rate of nucleation and the speed of growth during recrystallization[17]. This mechanism occurs due to an increased surface energy, which enables the boundaries to release particles, in the case of Nb precipitates (pinning effect)[18]. The segregation of Nb in solid solution to the grain boundaries reduces its mobility due to the drag effect. This effect is much more intense in Nb than in Ti[18].

Furthermore, during hot rolling, metallurgical and microstructural alterations occur very quickly, due to the extensive deformation and high temperature[19]. The morphology gradient of the grains observed in the 11CrTi steel was due to shear deformation between the work rolls and the surface

of the steel. This generates greater accumulated energy near the surface and, consequently, a greater driving force for recrystallization relative to the center. This accounts for the recrystallized condition of this area[20,21]. The 11CrTi+Nb steel, however, presented no recrystallized grains due to the effect of niobium, which delays the onset of recrystallization.

Although the two sheets of steel have very close contents of (Ti+Nb) in solid solution, the 11CrTi+Nb steel, with the higher contents of Nb in solution, does not recrystallize during hot rolling. The influence of Nb on recrystallization through the drag effect is higher than that of Ti, although both elements have a very close atomic radius. It is known that Nb alters the lattice parameter of the crystalline structure much more than does Ti, which is unrelated to the radius of the atoms. This effect is due to electronic interactions, although this is not yet fully understood. It should also be highlighted that the solubility of Nb in the ferritic structure is much lower than Ti[18], resulting in a more segregated Nb in the grain boundary, further reinforcing the drag effect.

The hot rolled sheet showed the heterogeneous texture along the thickness in both sheets of steel (Fig.1, and Fig.2). Raabe and Lücke[21] reported that heterogeneous texture occurs due to the thermal and deformation profile throughout the thickness. Near the surface, shear components are developed as results from shear deformation. The shear condition is weakened through the thickness, and the center is deformed by plain strain, leading to the formation α-fibers and γ-fibers. In addition, the {001}⟨011⟩ component present in the center region is related to development from the {001}//*N.D.* columnar grains, which grows quickly during solidifications on continuous casting[19,22].

The texture after cold rolling showed the main difference in the center region (Figure 5). It was observed that the γ-fiber was stronger in 11CrTi+Nb steel (Fig. 5d), while the α-fiber was more intense in the 11CrTi steel (Fig. 5b). As shown in Fig. 5b, the α-fiber was more intense in the center region than on the surface, which was more poorly developed. Among of the α-fibers, the {001}<110> components showed the highest intensity in the center region. This result suggests that this component was retained from the hot rolled sample. Furthermore, with the increase in deformation during cold rolling, the texture becomes more intense. In both steels, the {001}<110> Goss component was not observed (Fig. 5) after cold rolling. During the deformation, the {001}<110> Goss component can rotate toward {001}<110> on the α-fiber or {111}<112> on the γ-fiber[21]. Inagaki[23] reported the formation of γ-fibers by rotation along the following path: {110}<001>-{554}<225>-{111}<112>-{111}<110>-{223}<110>. This rotation contributed to an increase in the γ-fiber and to a disappearance of the shear textures. A similar deformation texture was also observed in other Ti and Nb-containing steels[24].

The recrystallization texture was notably different after annealing (Fig. 7). The 11CrTi+Nb steel presented the strongest γ-fiber and shifted components. The formation of the recrystallization texture depends on the orientation of the nuclei and their growth[25]. According to Hutchinson[26], the final texture should be dominant by the nuclei which form soonest and which are most numerous. Additionally, during the progress of nucleation, the γ-fiber grains have a high nucleation rate[25-27]. Gao et al.[28] reported {111}<112> nuclei at {111}<110> or vice versa. Thus, a high intensity of the γ-fiber after cold rolling favored its own formation after annealing. This trend was observed for the 11CrTi+Nb steel (Fig. 4d and Fig. 6b). The shifted components of the γ-fiber ideal have been reported in ferritic stainless steel. Sinclair et al.[29] cited that these components improve in intensity with increased levels of cold reduction. Siqueira et al.[30] reported the increase in the γ-fiber fraction with the increase in amounts of Nb during the secondary recrystallization in 16%Cr ferritic stainless steel. Shu at el.[6] cited that the Ti-addition in Nb-single stabilization steel promoted the intensification of the γ-fiber, especially in the {111}<112> component. In their study, the authors evaluated the effect of the 0.14%Ti-addition on 15%Cr and 0.31% Nb ferritic stainless steel.

The Nb-addition improved the average normal and planar anisotropy coefficients, as shown in table 3. This result is related to the greater γ/θ ratio in this steel. Studies have illustrated that for ferritic stainless steels, the higher fraction of γ-fiber improves the average normal coefficient of anisotropy, $\overline{R}$[28,31,32]. This is one of the most efficient forms of manufactured ferritic stainless steels with good deep drawability[31]. The value of the planar anisotropy coefficient, Δr, which was lower for 11CrTi+Nb steel, favors a lower trend to the formation of an earing during forming, indicating a higher performance material (Fig. 8).

5. Conclusions

- Recrystallization during the hot rolling process was less pronounced in Nb-Ti-stabilized steel when compared to the 11CrTi steel. The Nb-additon reduces the mobility of the boundaries due to the drag and pinning effect.
- Deformation texture showed α-fiber and γ-fiber developed after cold rolling. In the 11CrTi steel, the α-fiber was more pronounced due to its presence in the hot rolled sheets and deformation process. On the other hand, the high intensity of the {011}<100> Goss component in 11CrTi+Nb hot rolled favored the development of the γ-fiber after cold rolling.
- The γ-fiber was more intense in 11CrTi+Nb than in 11CrTi steel after annealing. Among the γ-fiber, the

{111}⟨121⟩ component was more developed. The Nb-addition and deformation texture contributed to the formation of higher γ-fiber.

- High average normal anisotropy was obtained in 11CrTi+Nb steel. The increase in γ-fiber was more favorable for deep drawing, illustrated by the better results obtained in the Swift test.

6. Acknowledgements

The authors wish to acknowledge Aperam South America, Fapemig, CNPq, and Capes-PROEX.

7. References

1. Franson IA, Fritz JD. Stabilization Requirements for T409 (UNS S40900) Ferritic Stainless Steel. SAE Technical Papers Series 971005. In: *SAE International Congress and Exposition*; 1997 Feb 24-27; Detroit, MI, USA.

2. Scalise C, de Oliveira MCL, Sayeg IJ, Antunes RA. Sensitization Behavior of Type 409 Ferritic Stainless Steel: Confronting DL-EPR Test and Practice W of ASTM A763. *Journal of Materials Engineering and Performance*. 2014;23(6):2164-2173.

3. Hiramatsu N. Niobium in Ferritic and Martensitic Stainless Steels. In: *Proceedings of the International Symposium Niobium 2001*; 2001 Dec 2-5; Orlando, FL, USA.

4. Cavazos JL. Characterization of precipitates formed in a ferritic stainless steel stabilized with Zr and Ti additions. *Materials Characterization*. 2006;56(2):96-101.

5. Tanure LPAR, de Alcântara CM, de Oliveira TR, Santos DB, Gonzalez BM. Comparison of Microstructure and Mechanical Behavior of the Ferritic Stainless Steels ASTM 430 Stabilized with Niobium and ASTM 439 Stabilized with Niobium and Titanium. *Materials Science Forum*. 2017;879:1651-1655.

6. Shu J, Bi H, Li X, Xu Z. Effect of Ti addition on forming limit diagrams of Nb-bearing ferritic stainless steel. *Journal of Materials Processing Technology*. 2012;212(1):59-65.

7. Yan H, Bi H, Li X, Xu Z. Microstructure and texture of Nb + Ti stabilized ferritic stainless steel. *Materials Characterization*. 2008;59(12):1741-1746.

8. ASTM International. *ASTM A240/A240M -12a - Standard Specification for Chromium and Chromium-Nickel Stainless Steel Plate, Sheet, and Strip for Pressure Vessels and for General Applications*. West Conshohocken: ASTM International; 2012.

9. ASTM International. *ASTM E112-13: Standard Test Methods for Determining Average Grain Size*. West Conshohocken: ASTM International; 2013.

10. Wright SI, Nowell MM, Field DP. A Review of Strain Analysis Using Electron Backscatter Diffraction. *Microscopy and Microanalysis*. 2011;17(3):316-329.

11. Lee KM, Huh MY, Engler O. Quantitative Analysis of Micro-Textures during Recrystallization in an Interstitial-Free Steel. *Steel Research International*. 2012;83(9):919-926.

12. Bunge HJ. *Texture Analysis in Materials Science - Mathematical Methods*. Oxford: Butterworth-Heinemann; 1982.

13. Hosford WF, Caddell RM. *Metal Forming: Mechanics and Metallurgy*. 4th ed. New York: Cambridge University Press; 2011.

14. ASTM International. *ASTM A370-16 - Standard Test Methods and Definitions for Mechanical Testing of Steel Products*. West Conshohocken: ASTM International; 2016.

15. ASTM International. *ASTM E517-00 (2010) - Standard Test Method for Plastic Strain Ratio r for Sheet Metal*. West Conshohocken: ASTM International; 2010.

16. Faria RA, Godefroid LB. Effect of Stabilization on Creep resistance of Ferritic Stainless Steels Used in Exhaust Systems. In: *19th International Congress of Mechanical Engineering (COBEM 2007)*. 2007 Nov 5-9; Brasília, DF, Brazil.

17. Abbaschian R, Abbaschian L, Reed-Hill RE. *Physical Metallurgy Principles*. 4th ed. Stanford: Cengage Learning; 2009. 769 p.

18. de Oliveira TR. *Effet du niobium et du titane sur la déformation à chaud d'aciers inoxydables ferritiques stabilisés*. [Thesis]. Saint-Étienne: Ecole Nationale Supérieure des Mines de Saint-Étienne; 2003.

19. Huh MY, Engler O. Effect of intermediate annealing on texture, formability and ridging of 17%Cr ferritic stainless steel sheet. *Materials Science and Engineering: A*. 2001;308(1-2):74-87.

20. Siqueira RP, Sandim HRZ, Oliveira TR, Raabe D. Composition and orientation effects on the final recrystallization texture of coarse-grained Nb-containing AISI 430 ferritic stainless steels. *Materials Science and Engineering: A*. 2011;528(9):3513-3519.

21. Raabe D, Lüucke K. Textures of ferritic stainless steels. *Materials Science and Technology*. 1993;9(4):302-312.

22. Braga FV, Escobar DP, Reis TJA, de Oliveira NJL, Andrade MS. Recrystallization of niobium stabilized ferritic stainless steel during hot rolling simulation by torsion tests. *Journal of Materials Research and Technology*. 2016;5(1):92-99.

23. Inagaki H. Fundamental Aspects of Texture Formation in Low Carbon Steel. *ISIJ International*. 1994;34(4):313-321.

24. de Abreu HFG, Bruno ADS, Tavares SSM, Santos RP, Carvalho SS. Effect of high temperature annealing on texture and microstructure on an AISI-444 ferritic stainless steel. *Materials Characterization*. 2006;57(4-5):342-347.

25. Humphreys FJ, Hatherly M. *Recrystallization and Related Annealing Phenomena*. 2nd ed. Oxford: Elsevier; 2004.

26. Hutchinson WB. Development and control of annealing textures in low-carbon steels. *International Metal Reviews*. 1984;29(1):25-42.

27. Ray RK, Jonas JJ, Hook RE. Cold rolling and annealing textures in low carbon and extra low carbon steels. *International Materials Reviews*. 1994;39(4):129-172.

28. Gao F, Liu Z, Liu H, Wang G. Texture evolution and formability under different hot rolling conditions in ultra purified 17%Cr ferritic stainless steels. *Materials Characterization*. 2013;75:93-100.

29. Sinclair CW, Mithieux JD, Schmitt JH, Bréchet Y. Recrystallization of stabilized ferritic stainless steel sheet. *Metallurgical and Materials Transactions A*. 2005;36(11):3205-3215.

30. Siqueira RP, Sandim HRZ, Oliveira TR. Texture evolution in Nb-containing ferritic stainless steels during secondary recrystallization. *Materials Science and Engineering: A*. 2008;497(1-2):216-223.

31. Yazawa Y, Ozaki Y, Kato Y, Furukimi O. Development of ferritic stainless steel sheets with excellent deep drawability by {1 1 1} recrystallization texture control. *JSAE Review*. 2003;24(4):483-488.

32. Gao F, Yu F, Misra RDK, Zhang X, Zhang S, Liu Z. Microstructure, Texture, and Deep Drawability Under Two Different Cold-Rolling Processes in Ferritic Stainless Steel. *Journal of Materials Engineering and Performance*. 2015;24(10):3862-3880.